LAWRENCE
LIVERMORE
NATIONAL
LABORATORY

UCRL-JRNL-234626

The total charm cross section

R. Vogt

September 14, 2007

European Physical Journal Special Topics

Updated October 14, 2003

EPJ manuscript No.
(will be inserted by the editor)

The total charm cross section

R. Vogt[1,2] [a]

[1] Lawrence Livermore National Laboratory, Livermore, CA, USA
[2] Department of Physics, UC Davis, Davis, CA, USA

Abstract. We assess the theoretical uncertainties on the total charm cross section. We discuss the importance of the quark mass, the scale choice and the parton densities on the estimate of the uncertainty. We conclude that the uncertainty on the total charm cross section is difficult to quantify.

1 Introduction

Open charm measurements date back to the late 1970s when D and $\overline{D}$ mesons were first detected, completing the picture of the fourth quark begun when the J/ψ was detected in pBe and e^+e^- interactions. The charm quark was postulated to have a mass between 1.2 and 1.8 GeV, within the regime of perturbative quantum chromodynamics (pQCD). Because of its relatively large mass, it is possible to calculate a total $c\overline{c}$ cross section, not the case for lighter flavors such as strangeness. Charm hadrons are usually detected two ways. The reconstruction of decays to charged hadrons such as $D^0 \to K^-\pi^+$ (3.8%) and $D^+ \to K^-\pi^+\pi^+$ (9.1%) gives the full momentum of the initial D meson, yielding the best direct measurement. Charm can also be detected indirectly via semi-leptonic decays to leptons such as $D \to Kl\nu_l$ although the momentum of the parent D meson remains unknown. Early measurements of prompt leptons in beam dump experiments assumed that the density of the dump was high enough to absorb semi-leptonic decays of non-charm hadrons, leaving only the charm component. At modern colliders, it is not possible to use beam dumps to measure charm from leptons but, at sufficiently high p_T, electrons from charm emerge from hadronic cocktails [1,2].

Although D mesons alone are often used to calculate the total $c\overline{c}$ cross section, other charm hadrons also exist. The excited D states, D^*s, decay primarily to charged and neutral D mesons. The charm-strange meson, the D_s, decays to charged hadrons and simultaneously to leptons. The lowest mass charm baryon is the Λ_c^+ which decays primarily to $\Lambda(uds)$ but also decays to $pK^-\pi^+$ (2.8%) and semi-leptonically with a 4.5% branching ratio. The heavier ground state charm baryons and their excited states (Σ_c and higher) decay through Λ_cs. The charm-strange baryons are assumed to be a negligible contribution to the total cross section.

Extracting the total charm cross section is a non-trivial task. To go from a finite number of measured D mesons in a particular decay channel to the total $c\overline{c}$ cross section one must: divide by the branching ratio for that channel; correct for the luminosity, $\sigma_D = N_D/\mathcal{L}t$; extrapolate to full phase space from the finite detector acceptance; divide by two to get the pair cross section from the single Ds; and multiply by a correction factor [3] to account for the unmeasured charm hadrons. There are assumptions all along the way. The most important is the extrapolation to full phase space. Before QCD calculations were available, the data were extrapolated assuming a power law for the x_F distribution, related to the longitudinal momentum of the charm hadron by $x_F = p_z/(\sqrt{S}/2) = 2m_T \sinh y/\sqrt{S}$. The canonical parameterization is $(1-x_F)^c$ where c was either fit to data over a finite x_F range or simply assumed. These parameterizations could lead to large overestimates of the total cross section when $0 < c < 2$ was assumed, especially

[a] e-mail: vogt2@llnl.gov

when data were taken only near $x_F = 0$. Lepton measurements were more conservative but were typically at more forward x_F.

Rather than assess the uncertainties in the data, here we address the theoretical uncertainties in the calculation of the charm and bottom cross sections. Since the data are generally taken in a finite kinematic region, we begin with the calculation of the inclusive distributions to the Fixed-Order Next-to-Leading Logarithm (FONLL) level and then discuss the total cross section calculations to next-to-leading order (NLO), the most accurate calculation of the total cross section.

We calculate the transverse momentum (p_T) distributions of charm and bottom quarks, the charm and bottom hadron distributions resulting from fragmentation and, finally, the electrons produced in semi-leptonic decays of the hadrons [4]. We then calculate the total charm and bottom cross sections, both by the integral over the inclusive p_T distribution and by integrating the total partonic cross section. At each step, we clarify the theoretical framework as well as the parameters and phenomenological inputs. Our final prediction is thus not a single number but rather an uncertainty band which has a reasonably large probability of containing the 'true' theoretical prediction. We show that applying this procedure blindly may lead to an apprent discrepancy in the two methods, particularly for charm production. We explain why this seems to be the case as well as why, when the calculations are done consistently, there is no discrepancy. The theoretical uncertainties in both methods of obtaining the total cross section are estimated as extensively as possible. We show that, for charm production, the theoretical uncertainty on the total cross section is difficult to quantify in a reliable way.

2 Total heavy flavor cross sections from integrated inclusive distributions

We first discuss how the total cross section and its accompanying uncertainty is obtained from inclusive single particle distributions. We begin with a description of the calculated single electron spectrum since heavy flavor hadrons are often observed through their semi-leptonic decays, particularly at colliders where direct reconstruction of heavy flavored hadrons at low p_T is difficult. Reconstructed D and B meson decays can only be used to obtain the total heavy flavor cross section if they are measured down to $p_T = 0$, difficult at colliders. However, STAR has reconstructed $D^0 \rightarrow K^{\pm}\pi^{\mp}$ decays to $p_T \sim 0$ in addition to their single electron measurement [1]. PHENIX has measured the single electron spectra from heavy flavor decays alone [2].

The theoretical prediction of the electron spectrum includes three main components: the p_T and rapidity distributions of the heavy quark Q in pp collisions at $\sqrt{S} = 200$ GeV, calculated in perturbative QCD; fragmentation of the heavy quarks into heavy hadrons, H_Q, described by phenomenological input extracted from e^+e^- data; and the decay of H_Q into electrons according to spectra available from other measurements. This cross section is schematically written as

$$\frac{Ed^3\sigma_e}{dp^3} = \frac{E_Q d^3\sigma_Q}{dp_Q^3} \otimes D(Q \rightarrow H_Q) \otimes f(H_Q \rightarrow e) \, , \tag{1}$$

where the symbol $\otimes$ denotes a generic convolution. The electron decay spectrum term $f(H_Q \rightarrow e)$ also implicitly accounts for the proper branching ratio.

The distribution $Ed^3\sigma_Q/dp_Q^3$ is evaluated at the FONLL level, implemented in Ref. [7]. In addition to including the full fixed-order NLO result [8,9], the FONLL calculation also resums [10] large perturbative terms proportional to $\alpha_s^n \log^k(p_T/m)$ to all orders with next-to-leading logarithmic (NLL) accuracy (i.e. $k = n$, $n-1$) where m is the heavy quark mass.

The perturbative parameters are the heavy quark mass and the value of the strong coupling, α_s, while the parton densities are a nonperturbative input. We take central values of 1.5 GeV for charm and 4.75 GeV for bottom as reference values and vary the masses between 1.3 and 1.7 GeV for charm and 4.5 and 5 GeV for bottom to estimate the resulting mass uncertainties.

Since the FONLL calculation treats the heavy quark as an active light flavor at $p_T >> m$, the number of light flavors used to calculate α_s includes the heavy quark, i.e. $n_{\rm lf} + 1$ where, for

charm, $n_{\rm lf} = 3$ (u, d and s). The same number of flavors, $n_{\rm lf}+1$, is also used in the fixed-order scheme where the quark mass is finite. However, in other fixed-order calculations, the number of light flavors is fixed to $n_{\rm lf}$. The QCD scale at five flavors, $\Lambda^{(5)}$, is set to 0.226 GeV, as in the CTEQ6M parton densities [11].

The perturbative calculation also depends on the unphysical factorization (μ_F) and renormalization (μ_R) scales. The sensitivity of the cross section to their variation can be used to estimate the perturbative uncertainty due to the absence of higher orders. We have taken $\mu_{R,F} = \mu_0 = \sqrt{p_T^2 + m^2}$ as a central value and varied the two scales independently within a 'fiducial' region defined by $\mu_{R,F} = \xi_{R,F}\mu_0$ with $0.5 \leq \xi_{R,F} \leq 2$ and $0.5 \leq \xi_R/\xi_F \leq 2$. In practice, we use the following seven sets: $\{(\xi_R, \xi_F)\} = \{$(1,1), (2,2), (0.5,0.5), (1,0.5), (2,1), (0.5,1), (1,2)$\}$. The envelope containing the resulting curves defines the uncertainty. Finally, the uncertainties stemming from mass and scale variations are added in quadrature.

The fragmentation functions, $D(c \to D)$ and $D(b \to B)$, where D and B indicate a generic admixture of charm and bottom hadrons, are consistently extracted from e^+e^- data in the context of FONLL [12]. Using the Peterson *et al.* fragmentation function [13], with standard parameter choices $\epsilon_c \simeq 0.06 \pm 0.03$ and $\epsilon_b \simeq 0.006 \pm 0.003$ does not provide a valid description of fragmentation to FONLL.

The measured spectra for primary $B \to e$ and $D \to e$ decays are modeled and assumed to be equal for all bottom and charm hadrons respectively. The contribution of electrons from secondary B decays, $B \to D \to e$, was obtained by convoluting the $D \to e$ spectrum with a parton-model prediction of $b \to c$ decay. The resulting electron spectrum is very soft, giving a negligible contribution to the total. The decay spectra are normalized using the branching ratios for bottom and charm hadron mixtures [14]: BR$(B \to e) = 10.86 \pm 0.35\%$, BR$(D \to e) = 10.3 \pm 1.2\%$, and BR$(B \to D \to e) = 9.6 \pm 0.6\%$.

We first present the transverse momentum distributions for charm and bottom quarks. Figure 1 shows the theoretical uncertainty bands for the two distributions, obtained by summing the mass and scale uncertainties in quadrature so that

$$\frac{d\sigma_{\rm max}}{dp_T} = \frac{d\sigma_C}{dp_T} + \sqrt{\left(\frac{d\sigma_{\mu,\rm max}}{dp_T} - \frac{d\sigma_C}{dp_T}\right)^2 + \left(\frac{d\sigma_{m,\rm max}}{dp_T} - \frac{d\sigma_C}{dp_T}\right)^2} \tag{2}$$

$$\frac{d\sigma_{\rm min}}{dp_T} = \frac{d\sigma_C}{dp_T} - \sqrt{\left(\frac{d\sigma_{\mu,\rm min}}{dp_T} - \frac{d\sigma_C}{dp_T}\right)^2 + \left(\frac{d\sigma_{m,\rm min}}{dp_T} - \frac{d\sigma_C}{dp_T}\right)^2}\,. \tag{3}$$

where C is the central values, μ, max (μ, min) is the maximum (minimum) cross section obtained by choosing the central value with the scale factors in our seven fiducial sets, and m, max (m, min) is the maximum (minimum) cross section obtained with $\xi_R = \xi_F = 1$ and the lower and upper limits on the quark mass respectively. There is, however, considerable arbitrariness in the choice of the method used to assess the theoretical uncertainties. In fact, the meaning of the theoretical error due to unknown higher order effects is, to a large extent, subjective. The recipe we follow is often used in calculations of cross sections at hadron colliders and is similar to the one used to compute heavy flavor cross sections at the Tevatron (see Refs. [15–17]). By experience, we assign a probability of 80-90% that the true result lies within the band.

Note that the charm quark uncertainty band is enlarged at low p_T due to the large value of α_s at low scales and the increased sensitivity of the cross section to the charm quark mass. In Ref. [4], we also noted that, due to the fairly hard fragmentation function, the D meson and c quark distributions begin to differ outside the uncertainty bands only for $p_T > 9$ GeV while the b quark and B meson bands overlap over all p_T.

The single electron uncertainty bands from $D \to e$, $B \to e$ and $B \to D \to e$ as well as the sum are compared to the STAR [1] and PHENIX [2] data on the right-hand side of Fig. 1. As expected, $B \to D \to e$ is a negligible contribution to the total. While $D \to e$ decays dominate at low p_T, the $B \to e$ contribution begins to dominate at higher p_T. The two uncertainty bands cross each other in the region $3.5 < p_T < 12$ GeV. The region of crossover is rather broad since we consider the c and b quark mass and scale uncertainties to be uncorrelated. If the scale

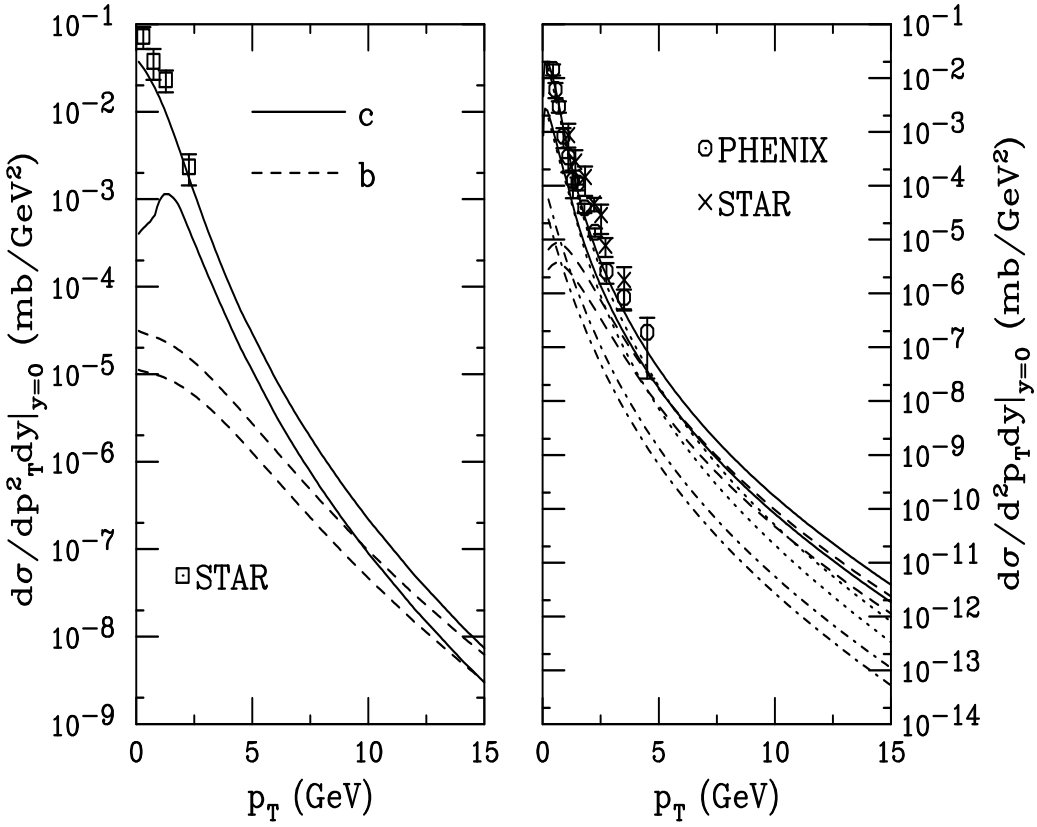

Fig. 1. Left-hand side: The FONLL p_T bands for c and b quark production compared to the STAR D meson data [1]. Right-hand side: The heavy flavor contributions to the single electron spectra: $D \to eX$ (dotted), $B \to lX$ (dashed), $B \to D \to lX$ (dot-dashed) and the sum (solid). is compared to the PHENIX [2] and STAR [1] data.

uncertainties were assumed to be correlated, the crossover region would be narrower, as shown in Ref. [5]. However, for a true measure of the uncertainty, we cannot assume that the scales are correlated. The PHENIX measurement is in relatively good agreement with the upper edge of the uncertainty band in Fig. 1 while the STAR data tend to lie a factor of 4-5 above the central value, falling well above the band.

If the distributions shown here are integrated over all phase space, the 'perturbative' inputs used in the calculation lead to a FONLL total $c\bar{c}$ cross section in pp collisions of

$$\sigma_{c\bar{c}}^{\rm FONLL} = 256^{+400}_{-146}\ \mu{\rm b} \tag{4}$$

at $\sqrt{S} = 200$ GeV. The corresponding NLO prediction is

$$\sigma_{c\bar{c}}^{\rm NLO} = 244^{+381}_{-134}\ \mu{\rm b}\ . \tag{5}$$

The theoretical uncertainty is evaluated as described above. Thus the two calculations are equivalent at the total cross section level within the large perturbative uncertainties, as expected. The total cross section for bottom production is

$$\sigma_{b\bar{b}}^{\rm FONLL} = 1.87^{+0.99}_{-0.67}\ \mu{\rm b}\ . \tag{6}$$

Because the FONLL and NLO distributions tend to coincide at small p_T and the total cross section is dominated by the low p_T region, the total cross sections and their uncertainties are nearly equal in the FONLL and NLO approaches. Earlier papers [6] used $m_c = 1.2$ GeV and

$\mu_R = \mu_F = 2\sqrt{p_T^2 + m^2}$ as reference parameters. With this choice we find $\sigma_{c\bar{c}}^{\rm NLO} = 427$ μb, within the calculated theoretical uncertainty band.

3 Total heavy flavor cross section from total partonic cross sections

The total partonic cross section has only been completely calculated to NLO [8]. Some NNLO calculations are available near threshold, applicable for $\sqrt{S} \leq 20 - 25$ GeV [18,19]. The NLO corrections to the leading order (LO) cross sections are relatively large, $K_{\rm th} = \sigma_{\rm NLO}/\sigma_{\rm LO} \sim 2 - 3$, depending on μ, m and the parton densities [20]. The NNLO corrections are about as large to next-to-next-to-leading logarithm [18] but decrease to less than $K_{\rm th}$ when subleading logs are included [19]. Scaling functions [8] proportional to logs of μ^2/m^2 are used to calculate the total cross section to NLO.

The hadronic cross section in pp collisions can be written as

$$\sigma_{pp}(S, m^2) = \sum_{i,j=q,\overline{q},g} \int dx_1\, dx_2\, f_i^p(x_1, \mu_F^2)\, f_j^p(x_2, \mu_F^2)\, \widehat{\sigma}_{ij}(s, m^2, \mu_F^2, \mu_R^2) \tag{7}$$

where x_1 and x_2 are the fractional momenta carried by the colliding partons and f_i^p are the proton parton densities. The partonic cross sections are

$$\begin{aligned} \widehat{\sigma}_{ij}(s, m, \mu_F^2, \mu_R^2) = \frac{\alpha_s^2(\mu_R^2)}{m^2} \Big\{ & f_{ij}^{(0,0)}(\rho) \\ & + 4\pi\alpha_s(\mu_R^2) \left[f_{ij}^{(1,0)}(\rho) + f_{ij}^{(1,1)}(\rho) \ln\left(\frac{\mu_F^2}{m^2}\right) \right] + \mathcal{O}(\alpha_s^2) \Big\} \end{aligned} \tag{8}$$

where $\rho = 4m^2/s$ and $f_{ij}^{(k,l)}$ are the scaling functions to NLO [8].

At small ρ, the $\mathcal{O}(\alpha_s^2)$ and $\mathcal{O}(\alpha_s^3)$ $q\overline{q}$ and the $\mathcal{O}(\alpha_s^2)$ gg scaling functions become small while the $\mathcal{O}(\alpha_s^3)$ gg and qg scaling functions plateau at finite values. Thus, at collider energies, the total cross sections are primarily dependent on the small x parton densities and phase space.

The total cross section does not depend on any kinematic variables, only on the quark mass, m, and the renormalization and factorization scales where now $\mu_{R,F} = \mu_0 = m$ is the central value. The heavy quark is always considered massive in the calculation of the total cross section. Thus, the number of light quark flavors, $n_{\rm lf}$, does not include the heavy quark, while the FONLL calculation uses $n_{\rm lf} + 1$ flavors since the heavy quark is an active flavor at high p_T, as described in Section 2.

The theoretical uncertainty on the total cross section is studied within the same fiducial region as the p_T distributions with the upper and lower limits of the uncertainty band determined as in Eqs. (2) and (3). The energy dependence of the charm and bottom total cross sections is shown in Figs. 2 and 3 respectively. The left-hand sides of the figures blow up the fixed-target and CERN ISR energy regime while the right-hand sides show the extrapolation of the cross sections to the collider regime. The central value of the band is indicated by the solid curve while the upper and lower edges of the band are given by the dashed curves. The dotted curves in Fig. 2 are calculated with $\mu_F = \mu_R = 2m$ and $m = 1.2$ GeV, used in Ref. [6]. Note that the charm uncertainty band broadens as the energy increases. The lower edge of the charm band grows more slowly with $\sqrt{S}$ above RHIC energies while the upper edge is compatible with the reported total cross sections at RHIC [1,2].

With $n_{\rm lf}$ light flavors and a fixed scale, the charm and bottom NLO total cross sections at $\sqrt{S} = 200$ GeV are

$$\sigma_{c\bar{c}}^{\rm NLO_{n_{lf}}} = 301^{+1000}_{-210}\ \mu{\rm b}\ , \tag{9}$$

$$\sigma_{b\bar{b}}^{\rm NLO_{n_{lf}}} = 2.06^{+1.25}_{-0.81}\ \mu{\rm b} \tag{10}$$

respectively. While the central values are only about 25% and 10% higher than the FONLL result given in the previous section, the uncertainty is considerably larger, especially for charm.

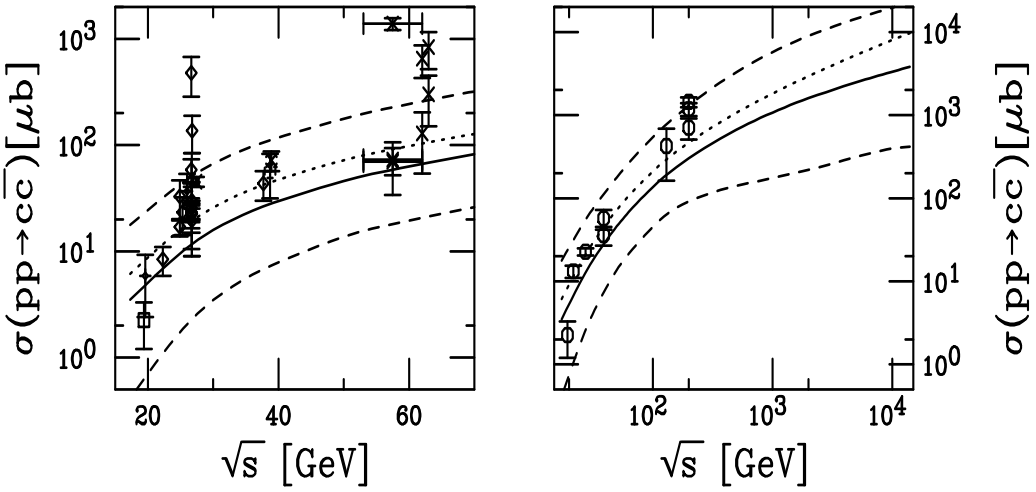

Fig. 2. The NLO total $c\bar{c}$ cross sections as a function of $\sqrt{S}$ for $\sqrt{S} \leq 70$ GeV (left-hand side) and up to 14 TeV (right-hand side) calculated with the CTEQ6M parton densities. The solid curve is the central result; the upper and lower dashed curves are the upper and lower edges of the uncertainty band. The dotted curves are calculations with $m = 1.2$ GeV, $\mu_F = \mu_R = 2m$.

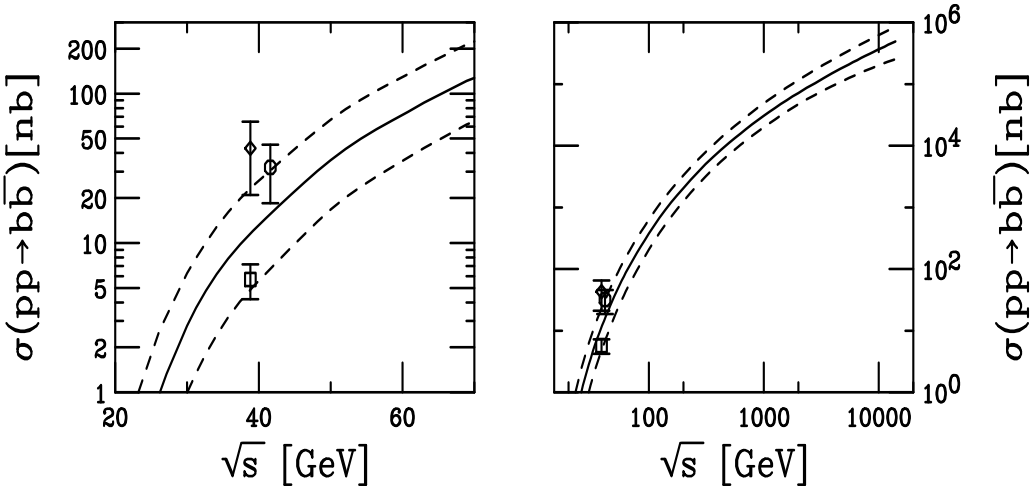

Fig. 3. The NLO total $b\bar{b}$ cross sections as a function of $\sqrt{S}$ for $\sqrt{S} \leq 70$ GeV (left-hand side) and up to 14 TeV (right-hand side) calculated with the CTEQ6M parton densities. The solid curve is the central result; the upper and lower dashed curves are the upper and lower edges of the uncertainty band.

We now discuss the major sources of the theoretical uncertainty and how the apparent discrepancy with the RHIC results in Section 2 comes about.

4 Comparison and discussion

From the results in the previous two sections, it seems that the total cross section is different depending on whether it is calculated from the integral over the inclusive p_T distribution or from the total partonic cross sections. The difference seems especially large for charm production. This is largely due to the way the strong coupling constant is calculated and the low x, low scale behavior of the parton densities.

Table 1. The values of α_s for charm and bottom production at the given values of $\xi_R = \mu_R/m$.

ξ_R	$n_{\rm lf} = 3$, $m = 1.5$ GeV	$n_{\rm lf} = 4$, $m = 4.75$ GeV
0.5	0.6688	0.2822
1	0.3527	0.2166
2	0.2547	0.1804

In this section, we discuss these two contributions to the theoretical uncertainty and show that, if the two calculations of the total cross section are done the same way, the two methods are, in fact, equivalent, as they should be.

The most trivial difference in the two calculations is that the p_T distribution is calculated with a running scale proportional to m_T while the total cross section is calculated with a fixed scale proportional to m. The charm quark uncertainty band is wider at low p_T, as shown in Fig. 1, because $p_T \leq m$ and the calculation is more sensitive to the lower scale in α_s since $m_T \sim m$ at low p_T. While it is more appropriate to use the running scale to calculate inclusive distributions, the difference between a fixed and a running scale can be checked by fixing the scale in the p_T distributions. The integral of the inclusive distribution increases about 20% for charm and about 10% for bottom when a fixed scale is used. This difference is approximately large enough to account for the difference in the central values of the total cross section.

One obviously important contribution to the uncertainty is the difference in the number of flavors in the two calculations, especially for charm since the fiducial range, $0.5 \leq \xi_R \leq 2$, is in a region where α_s is changing rapidly with μ_R. Although increasing the number of light flavors involves more than just changing a parameter in the calculation of α_s, we can get an estimate of the importance of the value of α_s to the uncertainty in the total cross section by looking at the dependence of α_s on the renormalization scale. When calculated with the 5 flavor QCD scale for CTEQ6M, $\Lambda_5 = 0.226$ MeV, and using a scheme where α_s is continuous across mass thresholds, we have the values shown in Table 1. It is clear, based on these values alone, that the charm uncertainty is larger than that for bottom since $\alpha_s(\xi_R = 0.5)/\alpha_s(\xi_R = 2) = 2.63$ for charm and 1.56 for bottom. The real difference in coupling strength between the two heavy quarks is even larger since the leading order cross section is proportional to α_s^2 while the next-order contribution is proportional to α_s^3.

Using $n_{\rm lf} + 1$ in the full calculation of the inclusive distributions reduces the uncertainty. When the total cross sections in Eqs. (4) and (5) are calculated with $n_{\rm lf}$, the uncertainty is increased so that the results are in agreement with that of Eq. (9).

Finally, we discuss the influence of the parton densities on the theoretical uncertainty. Since m is the only perturbative scale, the total cross section calculations in Section 3 are more sensitive to the low x and low μ behavior of the parton densities. Probing the full fiducial range of the uncertainty band is problematic for charm production since $\xi_F = 0.5$ is below the minimum scale of the CTEQ6M parton densities, $\mu_0^{\rm CTEQ6M} = 1.3$ GeV. Thus, for this scale, backward evolution of the parton densities is required.

The CTEQ6M (NLO, $\overline{\rm MS}$ scheme) gluon distributions in the fiducial region of the factorization scale, $0.5 \leq \xi_F \leq 2$, are shown in Fig. 4. The behavior of the gluon distributions for charm (left) and bottom (right) are quite different. Since the range $0.5m \leq \mu_F \leq 2m$ for bottom quarks lies well above $\mu_0^{\rm CTEQ6M}$, the scale dependence is as expected, with the gluon distribution increasing with decreasing x and with the highest low x gluon density at the largest scale. For x values larger than that of central rapidity at RHIC, the gluon densities are rather similar although the density at the lower scale is larger in the fixed-target regime. This x dependence is quite typical for large perturbative factorization scales and demonstrates why the bottom quark cross section is well behaved as a function of $\sqrt{S}$.

When the fixed factorization scale (in Eq. (7) is large enough, the lowest scales give the highest cross sections. The largest cross sections in the fixed-target regime are obtained with the combinations $(\xi_R, \xi_F) = (0.5, 0.5)$, (0.5,1) and (1,0.5). At relatively low $\sqrt{S}$, the slightly higher value of $\alpha_s(\xi_R = 0.5)$ compensates for the lower gluon density with $\xi_F = 1$ at large x so that the cross section with $(\xi_R, \xi_F) = (0.5, 1)$ is higher than that with (1,0.5). As the energy

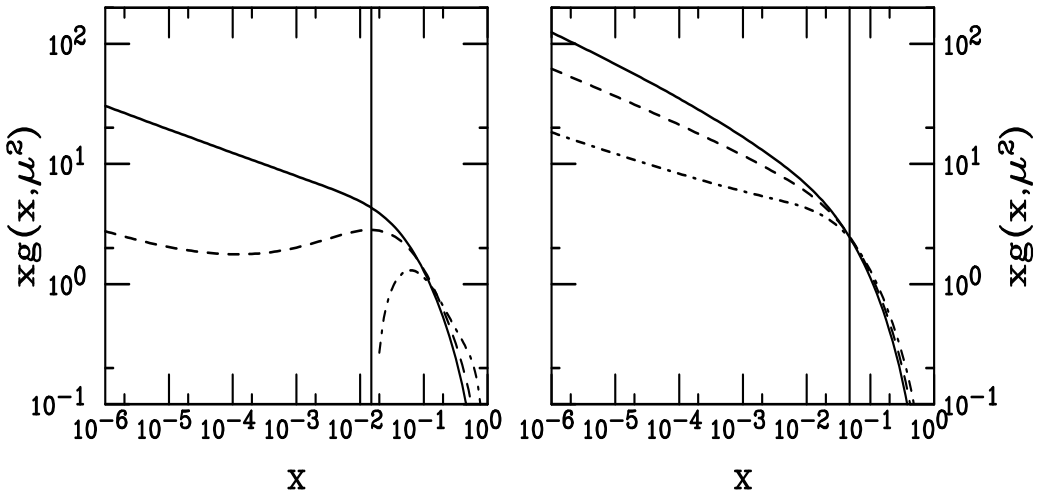

Fig. 4. The CTEQ6M parton densities as a function of x for $\xi = 0.5$ (dot-dashed), $\xi = 1$ (dashed) and $\xi = 2$ (solid) for $m = 1.5$ GeV (left-hand side) and 4.75 GeV (right-hand side). The vertical line is the value $x = 2m/\sqrt{S}$ in $\sqrt{S} = 200$ GeV pp collisions at RHIC.

increases and lower x values are probed, the lower small x gluon density with $\xi_F = 0.5$ can no longer overcome the difference between $\alpha_s(\xi_R = 1)$ and $\alpha_s(\xi_R = 0.5)$ and, at LHC energies, the cross section with $(\xi_R, \xi_F) = (1, 0.5)$ is smaller. Indeed, the lower factorization scale with $(\xi_R, \xi_F) = (0.5, 0.5)$ is not enough to keep the cross section with this parameter set larger than that with (1,0.5) or, for that matter, those with either or both $\xi_R, \xi_F = 2$ at sufficiently low x.

A similar effect occurs for $(\xi_R, \xi_F) = (2, 2)$, (2,1) and (1,2) except that now, at fixed-target energies, $(\xi_R, \xi_F) = (2, 2)$ gives the lowest cross section of the three pairs. In this case, $(\xi_R, \xi_F) = (1, 2)$ is the highest of the three since the gluon density with $\xi_F = 1$ is higher at large x (lower $\sqrt{S}$) and $\alpha_s(\xi_R = 1)$ is larger, compensating for the slightly lower gluon density at large x. At collider energies $(\xi_R, \xi_F) = (1, 2)$ remains the largest of these three parameter sets since the evolution at low x (large $\sqrt{S}$) is the dominant behavior. At large $\sqrt{S}$, the cross section with $(\xi_R, \xi_F) = (2, 1)$ drops below those calculated with the other two sets.

These subtle changes in which (ξ_R, ξ_F) set dominates the upper and lower limits of the bottom quark total cross section uncertainty band as a function of $\sqrt{S}$ do not significantly broaden the uncertainty band, even at the highest energies. This is because the factorization scale remains sufficiently above the minimum scale in the parton density.

The scale choice in the parton densities also affects the dominance of a particular parameter set (ξ_R, ξ_F) in the p_T distributions albeit to a lesser extent because at $p_T > m$ the scales are all large and perturbative. Different parameter sets dominate the p_T distribution because, at RHIC, high p_T probes the large x range of the gluon distribution. At $p_T \to 0$, the upper and lower edges of the band are determined by $(\xi_R, \xi_F) = (0.5, 1)$ and (1,0.5) respectively, as is also the case for the total cross sections. However, as p_T increases, the upper and lower edges of the band are defined by $(\xi_R, \xi_F) = (0.5, 0.5)$ and (2,2) respectively. Going to larger p_T has the same effect as moving to smaller $\sqrt{S}$, both probe larger x where the gluon distribution with $\xi_F = 0.5$ is higher than that with $\xi_F = 2$, as is obvious from the right-hand side of Fig. 4.

Even though the scale dependence of bottom production is not negligible, as we have seen, the dependence is not strong in the defined fiducial range. The difference in the $b\overline{b}$ cross sections in Eqs. (6) and (10) can be almost entirely attributed to the difference between the running scale in Eq. (1) and the fixed scale in Eq. (7). Thus the bottom production cross section is rather well under control.

However, the dependence of the total charm cross section on $\sqrt{S}$ is another story due to the behavior of the CTEQ6M gluon distribution at charm quark scales. The proximity of the charm quark mass to $\mu_0^{\rm CTEQ6M}$ makes the application of the full fiducial region to the estimate

of the theoretical uncertainty on the total charm cross section problematic. The smaller charm mass exaggerates the factorization scale dependence of the total cross section described above for bottom production.

The gluon distributions with $\xi_F = 2$ for charm and $\xi_F = 0.5$ for bottom are similar because the values of μ_F are nearly the same: 3 GeV and 2.375 GeV respectively. Thus at the highest value of ξ_F for charm, the gluon density at low x is well behaved. However, the behavior at lower scales is quite different, especially for $x < 10^{-2}$. When $\xi_F = 1$, the dashed curve on the left-hand side of Fig. 4 is no longer increasing with decreasing x but, instead, starts to dip and turn over. If fact, for $\xi_F = 0.5$, lower x values are not shown because the backwards evolution gives $xg(x, \xi_F = 1) = 0$, accounting for the high $\sqrt{S}$ behavior of the lower bound on the uncertainty band. The low μ_F behavior of the gluon density is very dependent on the choice of parton density because the groups making global parton density analyses all deal with extrapolations to unmeasured regions differently. All that is required is minimization of the global χ^2 and momentum conservation.

Thus the charm quark uncertainty band on the total cross section, Fig. 2 spans an order of magnitude at fixed-target energies, increasing to the value given in Eq. (9) for $n_{\rm lf}$ at $\sqrt{S} = 200$ GeV. The low scale behavior for $(\xi_R, \xi_F) = (0.5, 1)$ and (1,0.5) defines the upper and lower edges respectively of the uncertainty band at collider energies in all cases. Indeed, for the total cross section calculated with $n_{\rm lf}$ light quark flavors, the STAR point [1] is compatible with the upper limit of the band although the inclusive p_T data, with $n_{\rm lf} + 1$ light flavors, lies above it [21].

The charm band grows broader with increasing $\sqrt{S}$, corresponding to decreasing x. At 10 TeV, the width of the uncertainty band has increased to almost two orders of magnitude. Thus, without a better handle on the gluon density at low x and low scales, one may question whether such a large uncertainty is meaningful. It may also be questionable whether the lowest scales, ξ_R and $\xi_F = 0.5$ should be included in the calculation of the uncertainty when $\mu_F = 0.5m < \mu_0^{\rm CTEQ6M}$ for charm.

Even though the full fixed-target data set also exhibits a large uncertainty due to the method of extrapolation used and the assumed branching ratios and A dependence, as shown on the left-hand side of Fig. 2, if only more recent data are used, the uncertainty in the data seems to be reduced. As an alternative, one may try to 'fit' the mass and scale parameters to these data [6]. The dotted curves in Fig. 2 show the energy dependence of one such attempt with $m = 1.2$ GeV, $(\xi_R, \xi_F) = (2, 2)$. The calculation lies just above the central value of the band and, although the quark mass is smaller than the assumed central mass value, the larger value of ξ_F guarantees a more regular $\sqrt{S}$ dependence than that obtained with smaller values, as shown in Fig. 4.

5 Conclusions

We have shown that when the total cross section is calculated with the same parameter sets and the same number of light quark flavors, a consistent result is obtained by both integrating over an inclusive distribution and starting from the total partonic cross section, as should be expected. While this is true, the charm results are extremely sensitive to the number of flavors, the scale choice and the parton densities. One of the biggest sources of uncertainty in the total charm cross section at collider energies is the behavior of the gluon density at low x and low scale, as yet not well determined. Until it is further under control, better limits on the charm quark total cross section will be difficult to set.

It is thus not clear which estimate of the total charm cross section uncertainty is more reliable. If the low p_T region is ignored and the heavy quark may be considered an active flavor then the appropriate number of flavors is $n_{\rm lf} + 1$ rather than $n_{\rm lf}$ and the smaller error band used to compare the RHIC p_T distributions [21] is more reasonable. However, when heavy flavor production is measured over the full p_T range, down to $p_T \sim 0$, then three light flavors should likely be used for charm, resulting in the larger uncertainty. Unfortunately, in this case, the uncertainty is driven by scales lower than the initial scale of the parton density,

further complicating the interpretation of the limits on the uncertainty band. Thus, rather than arbitrarily choosing one result over another, we prefer to stress that there is little predictive power in the charm production uncertainty.

Acknowledgements

I am very pleased to contribute to this volume in honor of Prof. Zimanyi. I would like to thank him for introducing me to Budapest and Hungarian culture. From my very first trip to Budapest, Joszo and Magda were very kind to me, making sure I saw something besides the interior of the laboratory. Thanks to Joszo and his very active group, I have enjoyed many visits over the years and look forward to more in the future.

I would like to thank M. Cacciari, G. Odyniec and T. Ullrich for discussions. This work was performed under the auspices of the U.S. Department of Energy by University of California, Lawrence Livermore National Laboratory under Contract W-7405-Eng-48 and was also supported in part by the National Science Foundation Grant NSF PHY-0555660.

References

1. J. Adams *et al.* [STAR Collaboration], Phys. Rev. Lett. **94** (2005) 062301 [arXiv:nucl-ex/0407006].
2. A. Adare *et al.* [PHENIX Collaboration], Phys. Rev. Lett. **97** (2006) 252002 [arXiv:hep-ex/0609010]; S. S. Adler S S *et al.* [PHENIX Collaboration], (2006) *Preprint* nucl-ex/0609032
3. S. Frixione, M. L. Mangano, P. Nason and G. Ridolfi, Adv. Ser. Direct High Energy Phys. (1998) **15** 609.
4. M. Cacciari, P. Nason and R. Vogt, Phys. Rev. Lett. **95** (2005) 122001.
5. M. Djordjevic, M. Gyulassy, R. Vogt and S. Wicks, Phys. Lett. B **632** (2005) 81 [arXiv:nucl-th/0507019].
6. R. Vogt [Hard Probe Collaboration], Int. J. Mod. Phys. E **12** (2003) 211 [arXiv:hep-ph/0111271].
7. M. Cacciari, M. Greco and P. Nason, JHEP **9805** (1998) 007 [arXiv:hep-ph/9803400]; M. Cacciari, S. Frixione and P. Nason, JHEP **0103** (2001) 006 [arXiv:hep-ph/0102134].
8. P. Nason, S. Dawson and R. K. Ellis, Nucl. Phys. B **303** (1988) 607; P. Nason, S. Dawson and R. K. Ellis, Nucl. Phys. B **327** (1989) 49 [Erratum-ibid. B **335** (1990) 260].
9. W. Beenakker, W. L. van Neerven, R. Meng, G. A. Schuler and J. Smith, Nucl. Phys. B **351** (1991) 507.
10. M. Cacciari and M. Greco, Nucl. Phys. B **421** (1994) 530 [arXiv:hep-ph/9311260].
11. J. Pumplin *et al.*, *JHEP* **0207** (2002) 012 [arXiv:hep-ph/0201195]; D. Stump *et al.*, *JHEP* **0310** (2003) 046 [arXiv:hep-ph/0303013].
12. M. Cacciari and P. Nason, Phys. Rev. Lett. **89** (2002) 122003 [arXiv:hep-ph/0204025].
13. C. Peterson, D. Schlatter, I. Schmitt and P. M. Zerwas, Phys. Rev. D **27** (1983) 105.
14. S. Eidelman *et al.* [Particle Data Group Collaboration], Phys. Lett. B **592** (2004) 1.
15. M. Cacciari, S. Frixione, M. L. Mangano, P. Nason and G. Ridolfi, JHEP **0407** (2004) 033 [arXiv:hep-ph/0312132].
16. M. Cacciari and P. Nason, JHEP **0309** (2003) 006 [arXiv:hep-ph/0306212].
17. M. Cacciari, S. Frixione, M. L. Mangano, P. Nason and G. Ridolfi, JHEP **0404** (2004) 068 [arXiv:hep-ph/0303085].
18. N. Kidonakis, E. Laenen, S. Moch and R. Vogt, Phys. Rev. D **67** (2003) 074037 [arXiv:hep-ph/0212173].
19. N. Kidonakis and R. Vogt, Eur. J. Phys. C **36** (2004) 201 [arXiv:hep-ph/0401056].
20. R. Vogt, Heavy Ion Phys. **17** (2003) 75 [arXiv:hep-ph/0207359].
21. A. A. P. Suaide, J. Phys. G **34** (2007) 369 [arXiv:nucl-ex/0702035].